

# Gravitational Imprints from Heavy Kaluza-Klein Resonances

Eugenio Megías,<sup>1,\*</sup> Germano Nardini,<sup>2,†</sup> and Mariano Quirós<sup>3,‡</sup>

<sup>1</sup>*Departamento de Física Atómica, Molecular y Nuclear and Instituto Carlos I de Física Teórica y Computacional, Universidad de Granada, Avenida de Fuente Nueva s/n, 18071 Granada, Spain*

<sup>2</sup>*Faculty of Science and Technology, University of Stavanger, 4036 Stavanger, Norway*

<sup>3</sup>*Institut de Física d'Altes Energies (IFAE), The Barcelona Institute of Science and Technology (BIST), Campus UAB, 08193 Bellaterra (Barcelona) Spain*

(Dated: November 14, 2021)

We systematically study the holographic phase transition of the radion field in a five-dimensional warped model which includes a scalar potential with a power-like behavior. We consider Kaluza-Klein (KK) resonances with masses  $m_{\text{KK}}$  at the TeV scale or beyond. The backreaction of the radion field on the gravitational metric is taken into account by using the superpotential formalism. The confinement/deconfinement first order phase transition leads to a gravitational wave stochastic background. Its power spectrum peaks at a frequency that depends on the amount of tuning required in the electroweak sector. It turns out that the present and forthcoming gravitational wave observatories can probe scenarios where the KK resonances are very heavy. Current aLIGO data already rule out vector boson KK resonances with masses in the interval  $m_{\text{KK}} \sim (1-10) \times 10^5$  TeV. Future gravitational experiments will be sensitive to resonances with masses  $m_{\text{KK}} \lesssim 10^5$  TeV (LISA),  $10^8$  TeV (aLIGO Design) and  $10^9$  TeV (ET). Finally, we also find that the Big Bang Nucleosynthesis bound in the frequency spectrum turns into a lower bound for the nucleation temperature as  $T_n \gtrsim 10^{-4} \sqrt{N} m_{\text{KK}}$ .

The Standard Model is unable to explain some experimental observations (e.g. dark matter, the baryon asymmetry of the universe), and suffers from theoretical drawbacks (e.g. strong sensitivity to high scale physics, a.k.a. hierarchy problem). A warped extra dimension is a way of solving the hierarchy problem and relate the Planck scale  $M_P$  to the low energy scale  $\rho$ , which determines the spectrum of heavy resonances and is usually considered at the TeV scale [1, 2]. However, the elusiveness of experimental data on the search of stable narrow resonances [3, 4] is perhaps suggesting us that nature might not be as generous as we assumed it to be, and is not solving the “whole” hierarchy problem but only part of it, in which case  $\rho$  can be much heavier than the TeV scale worsening the little hierarchy problem.

But if nature had chosen that way, where could we find sensitivity to such a heavy physics, aside from future more energetic colliders? The answer is based on the presence of the only extra light field in the theory, the radion, which experiences a first order phase transition, the confinement/deconfinement transition, which generates a stochastic gravitational wave background (SGWB) detectable at the present and future interferometers [5–7]. In this paper we cover this issue for the minimal 5D warp model [1] with a stabilizing field with a bulk polynomial potential. Studies of the holographic phase transition have been performed with great detail in the literature [8–20]. Here we will take into account the full backreaction of the scalar field on the gravitational metric, using the superpotential mechanism and methods pro-

posed in Ref. [18], and consider the possibility of large enough values for the  $\rho$  parameter, while keeping an explanation of the hierarchy between  $M_P$  and  $\rho$  by means of the metric warp factor.

*The model.* We consider a scalar-gravity system, with metric  $g_{MN}$  defined in proper coordinates by  $ds^2 = g_{MN} dx^M dx^N \equiv e^{-2A(r)} \eta_{\mu\nu} dx^\mu dx^\nu - dr^2$ , and two branes at  $r = r_a$ , where  $a = 0, 1$  for the UV and IR brane, respectively. We fix  $r_0 = 0$  by convention, and our notation follows Ref. [18].

The background equations of motion (EoM) can be expressed in terms of the superpotential  $W(\phi)$  as [21]

$$\begin{aligned} \phi'(r) &= \frac{1}{2} W'(\phi), & A'(r) &= \frac{\kappa^2}{6} W(\phi), \\ V(\phi) &= \frac{1}{8} [W'(\phi)]^2 - \frac{\kappa^2}{6} W^2(\phi), \end{aligned} \quad (1)$$

where the prime symbol ( $'$ ) stands for the derivative of a function with respect to its argument, and  $\kappa^2 \equiv 1/(2M^3)$ , with  $M$  the 5D Planck mass.  $W$  is expressed as the expansion  $W = \sum_n s^n W_n$  [18, 22–24] where

$$W_0(\phi) = \frac{6}{\ell \kappa^2} + \frac{u}{\ell} \phi^2, \quad (2)$$

with  $\ell$  being a  $\mathcal{O}(M^{-1})$  parameter,  $u$  being dimensionless, and  $s$  playing the role of the (small) integration constant of Eq. (1). We work to linear approximation in  $s$  and keep the leading terms of the  $u \ll 1$  limit, for which one can solve the hierarchy problem with  $\mathcal{O}(1)$  values for  $v_a$ . We assume stiff potentials in the UV and IR branes inducing the boundary conditions  $\phi(r_a) = v_a$  [2].

To linear order  $W = W_0 + sW_1$  the superpotential is

$$W_1(\phi) = \frac{1}{\ell \kappa^2} \left( \frac{\phi}{v_0} \right)^{4/u} e^{\kappa^2(\phi^2 - v_0^2)/3}. \quad (3)$$

\* emegias@ugr.es

† germano.nardini@uis.no

‡ quiros@ifae.es

Similarly  $\phi$  can be decomposed as  $\phi = \phi_0 + s\phi_1$  with  $\phi_0(r) = v_0 e^{ur/\ell}$  and

$$\bar{\phi}_1(r) = \frac{1}{2u\bar{v}_0} e^{u\bar{r}} \left[ e^{(4-2u)\bar{r}} e^{\bar{v}_0^2/3(e^{2u\bar{r}}-1)} - 1 \right], \quad (4)$$

which fulfills the UV boundary condition  $\phi(r_0) = v_0$  [18]. The IR boundary condition  $\phi(r_1) = v_1$  requires

$$s(\bar{r}_1) = \frac{2u\bar{v}_0^2 e^{-u\bar{r}_1} \left( e^{u\bar{r}_1^0} - e^{u\bar{r}_1} \right)}{e^{(4-2u)\bar{r}_1} e^{\bar{v}_0^2/3(e^{2u\bar{r}_1}-1)} - 1}. \quad (5)$$

For convenience we have introduced the dimensionless quantities  $\bar{v}_a \equiv \kappa v_a$ ,  $\bar{\phi}(r) \equiv \kappa\phi(r)$ ,  $\bar{r} \equiv r/\ell$ ,  $\bar{r}_a \equiv r_a/\ell$ .

Likewise the expansion of the metric exponent,  $A(r) = A_0(r) + sA_1(r)$ , yields

$$A_0(r) = \bar{r} + \frac{\bar{v}_0^2}{12} (e^{2u\bar{r}} - 1), \quad (6)$$

$$A_1(r) = \frac{1}{12} \left[ e^{4A_0(\bar{r})} - 1 \right] + \frac{2+u}{24u} \left( 1 - \frac{\bar{v}_0^2}{\bar{v}_0^2} \right). \quad (7)$$

The effective potential. We define the effective potential normalized to its value at  $r_1 \rightarrow \infty$  as [18]

$$U_{\text{eff}}(r_1) = [\Lambda_1 + W_0(v_1)] e^{-4A_0(r_1)} [1 - 4A_1(r_1)s(r_1)] + s(r_1) \left[ e^{-4A_0(r_1)} W_1(v_1) - W_1(v_0) \right], \quad (8)$$

where  $\Lambda_1$  is the tension at the IR brane. We can tune to zero the first term of Eq. (8) by fixing  $\Lambda_1 = -W_0(v_1)$ . Consequently the leading-order dimensionless effective potential  $\bar{U}_{\text{eff}}^0(r_1) \equiv \ell\kappa^2 U_{\text{eff}}^0(r_1)$  is given by

$$\bar{U}_{\text{eff}}^0(\bar{r}_1) = 2u^2\bar{v}_1^2(\bar{r}_1^0 - \bar{r}_1) \left[ e^{4A_0(\bar{r}_1^0) - 4A_0(\bar{r}_1)} - 1 \right] e^{-4A_0(\bar{r}_1)}, \quad (9)$$

where  $\bar{r}_1^0$  comes from  $v_1 \equiv v_0 e^{u\bar{r}_1^0}$ . Note that  $A_0(\bar{r}_1)$  is a positive increasing function for  $\bar{r}_1 > 0$ , and thus the factor  $(\bar{r}_1^0 - \bar{r}_1)$  and the term inside the bracket have the same sign for any  $r_1$ . The potential in Eq. (9) is therefore positive definite. Moreover, one can see that  $\bar{U}_{\text{eff}}^0(\bar{r}_1)$  has degenerate minima, at  $\bar{r}_1 = \bar{r}_1^0$  and  $\bar{r}_1 \rightarrow \infty$ , where it vanishes. For the sake of comparison, the Goldberger-Wise potential of Ref. [2] writes in our notation

$$\bar{U}_{\text{eff}}^{\text{0GW}}(\bar{r}_1) = 4\bar{v}_0^2 e^{-4\bar{r}_1} \left( e^{u\bar{r}_1^0} - e^{-u\bar{r}_1} \right)^2 + \mathcal{O}(u) \quad (10)$$

which is positive definite when ignoring the  $\mathcal{O}(u)$  terms.

Fig. 1 displays the plot of the effective potential in Eq. (9) for parameter values leading to a potential minimum at  $\bar{r}_1^0 = 36$ . The expansion hierarchy  $s(\bar{r}_1)W_1(\bar{r}_1)/W_0(\bar{r}_1) \sim \mathcal{O}(10^{-4})$ , so the  $s$ -expansion of the superpotential converges fast. For the sake of comparison Fig. 1 also shows  $\bar{U}_{\text{eff}}^{\text{0GW}}$ , as well as  $\bar{U}_{\text{eff}}^0$  in the limit of no backreaction on the metric, i.e. considering  $A_0(r) \simeq \bar{r}$ .

Due to the above ‘‘tuning’’, the potential minima at  $\bar{r}_1 = (\bar{r}_1^0, \infty)$  are degenerate. This prevents the necessary

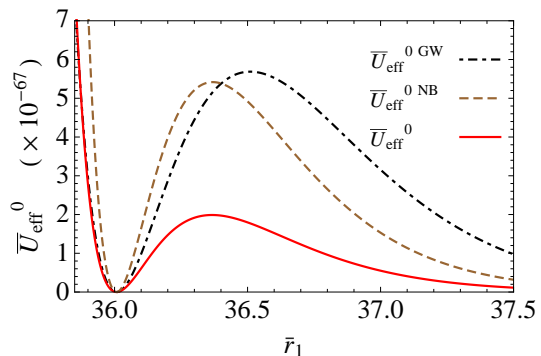


FIG. 1. The potential  $\bar{U}_{\text{eff}}^0$  in Eq. (9) (solid line), the same potential when neglecting the backreaction  $\bar{U}_{\text{eff}}^{\text{0NB}}$  (dashed line), and  $\bar{U}_{\text{eff}}^{\text{0GW}}$  in Eq. (10) (dashed-dotted line) as functions of  $\bar{r}_1$ . The plot assumes  $\bar{v}_0 = 1$ ,  $\bar{v}_1 = 2$ ,  $u = 0.0192$ .

transition from the deconfined phase in the early universe. To allow it, we relax the aforementioned tuning by the parameter  $\lambda_1 \equiv (\Lambda_1 + W_0(v_1))\ell\kappa^2/6$ . It follows

$$\bar{U}_{\text{eff}}(\bar{r}_1) \simeq \bar{U}_{\text{eff}}^0(\bar{r}_1) + 6\lambda_1 e^{-4A_0(\bar{r}_1)}, \quad (11)$$

where the term  $4A_1(\bar{r}_1)s(\bar{r}_1) \lesssim 10^{-3}$  is omitted. For  $\lambda_1 < 0$  the global minimum is at a finite value of  $r_1$ . The positions of the minima of  $\bar{U}_{\text{eff}}^0(r_1)$  in Eq. (9) and of  $\bar{U}_{\text{eff}}(\bar{r}_1)$  in Eq. (11) differ by a small amount  $\delta$ . By denoting the former as  $\bar{r}_1^m$  and plugging their difference  $\delta = \bar{r}_1^m - \bar{r}_1^0$  into Eq. (11), one finds

$$\delta \simeq -\frac{1}{4}\mathcal{W} \left[ -\frac{6\lambda_1}{u^2\bar{v}_1^2} \right], \quad (12)$$

where  $\mathcal{W}$  is the Lambert  $\mathcal{W}$  function and the result relies on the expansion  $u \ll 1$ , whose approximation holds within a few per mille. Using the formalism of [18] we find, to leading approximation in  $u$ , the radion field  $\bar{\chi}(r_1) \equiv \ell\chi(r_1)$  as  $\bar{\chi}(r_1) \simeq e^{-A_0(r_1)}$  which, once inverted, yields

$$\bar{r}_1(\bar{\chi}) = -\log \bar{\chi} + \frac{\bar{v}_0^2}{12} - \frac{1}{2u} \mathcal{W} \left[ \frac{u\bar{v}_0^2}{6} e^{u(\bar{v}_0^2/6 - 2\log \bar{\chi})} \right]. \quad (13)$$

A convenient parametrization of the (dimensionful) effective potential in units of the physically relevant parameter  $\rho \equiv e^{-A_0(\bar{r}_1^m)}/\ell$  is then

$$U_{\text{eff}}(\bar{r}_1) = \frac{N^2\rho^4}{8\pi^2} e^{4A_0(\bar{r}_1^m)} \bar{U}_{\text{eff}}(\bar{r}_1), \quad (14)$$

where  $N^2 = 8\pi^2\ell^3/\kappa^2$ .

Hence the radion has the potential  $V_{\text{rad}}(\chi) \equiv U_{\text{eff}}[\bar{r}_1(\bar{\chi})]$  with minimum at  $\langle \chi \rangle = \rho$ . Its mass can be computed from the radion EoM following [25]. In the limit of stiff brane potentials, the result for  $\bar{v}_0 = 1$ ,  $\bar{v}_1 = 2$  and  $\rho = 1$  (100) TeV is  $m_{\text{rad}}/\rho \simeq 0.10$  (0.12). For  $\bar{v}_0 = 0.1$ ,  $\bar{v}_1 = 0.2$ , where the backreaction on the metric is smaller, the radion is much lighter,  $m_{\text{rad}}/\rho \simeq 0.011$  (0.013) with  $\rho = 1$  (100) TeV, as expected. Using similar

approaches, we compute the mass of the first KK resonance for gauge bosons, obtaining  $m_{\text{KK}}/\rho \simeq 2.46$  (2.43) for  $\bar{v}_0 = 1, \bar{v}_1 = 2$  ( $\bar{v}_0 = 0.1, \bar{v}_1 = 0.2$ ), values almost independent of  $\lambda_1$  and  $\rho$ .

For concreteness, hereafter we assume  $\bar{v}_0 = 1, \bar{v}_1 = 2$  and  $\ell$  nearby the Planck length  $\ell_P$ , namely  $1/\ell = 10^{18} \text{ GeV} \simeq 0.4/\ell_P$ . In this way  $\rho$  is determined mainly by  $u$  and, with a milder dependence, by  $\lambda_1$ . We find the benchmark values  $u \simeq 0.0192$  (0.0219) for  $\rho = 1$  (100) TeV.

*The confinement/deconfinement phase transition.* It is the radion phase transition from its symmetric (deconfined) phase, at  $\chi = 0$ , to its broken (confined) phase, at  $\chi = \langle \chi \rangle \neq 0$ . At finite temperature the warped model admits an additional gravitational solution with a black hole (BH) singularity located at the event horizon  $r = r_h$  [8, 26],  $ds_{\text{BH}}^2 = -h(r)^{-1}dr^2 + e^{-2A(r)}(h(r)dt^2 - d\vec{x}^2)$ . Here  $h(r)$  is the blackening factor satisfying the boundary and regularity conditions  $h(0) = 1$  and  $h(r_h) = 0$ .

A solution of the EoM [18] provides the function  $h(r)$ , in the  $u \ll 1$  limit, as  $h(r) \simeq 1 - e^{4[A_0(r) - A_0(r_h)]}$ , which translates into  $\ell h'(r_h) \simeq -4$  since  $A'_0(r) = 1 + \mathcal{O}(u)$ . Thus the Hawking temperature,  $T_h$ , and the minimum of the free energy in the BH solution,  $F^{\text{BH}}(T_h)$ , read as

$$\ell T_h \equiv \bar{T}_h \simeq \frac{1}{\pi} e^{-A_0(r_h)}, \quad F_{\text{min}}^{\text{BH}}(T) \simeq -\frac{\pi^4 \ell^3}{\kappa^2} T^4. \quad (15)$$

In fact the free energy in the deconfined,  $F_d(T)$ , and confined,  $F_c(T)$ , phases at high temperature are given by

$$F_d = E_0 + F_{\text{min}}^{\text{BH}} - \frac{\pi^2}{90} g_d^{\text{eff}} T^4, \quad F_c = -\frac{\pi^2}{90} g_c^{\text{eff}} T^4, \quad (16)$$

where  $g_{d/c}^{\text{eff}}$  is the number of relativistic degrees of freedom in the deconfined/confined phase and  $E_0 = V_{\text{rad}}(0) - V_{\text{rad}}(\rho)$  is the potential gap between the two phases in the  $T = 0$  limit.

Below the critical temperature  $T_c$ , defined by  $F_c(T_c) = F_d(T_c)$ , the phase transition can start. We will assume  $g_d^{\text{eff}}(T_c) \simeq g_c^{\text{eff}}(T_c)$ <sup>1</sup>, and thus the critical temperature can be estimated as  $\pi T_c/\rho \simeq e^{A_0(\bar{r}_1^m)} |\bar{U}_{\text{eff}}(\bar{r}_1^m)|^{1/4}$ . We find that  $T_c/\rho$  is mostly insensitive to the particular value of  $u$  in the parameter region considered in this work.

The (first order) phase transition proceeds through bubble nucleation of the confined phase in the deconfined sea. The onset of the transition occurs at the nucleation temperature  $T_n < T_c$ . To compute  $T_n$  we calculate the Euclidean actions  $S_3/T$ , with symmetry  $O(3)$  (at high temperature), and  $S_4$ , with symmetry  $O(4)$  (at low temperature), and compare them with the expansion rate of

the universe at the corresponding temperature. Although we expect, on general grounds, the bubble formation to be dominated by thick wall approximation, at least for  $T_n \ll T_c$  [9, 13], we find that this approximation often mismatches the fully numerical result. We thus compute  $S_3/T$  and  $S_4$  via the numerical method introduced in [11, 18], and subsequently obtain  $T_n$  from the condition

$$S_E(T_n) \simeq 4 \log \frac{M_p/\rho}{T_n/\rho} \quad \text{with} \quad S_E = \min \left[ \frac{S_3(T_n)}{T_n}, S_4(T_n) \right].$$

The Euclidean actions scale as  $N^2$  so that they diverge in the limit  $N \rightarrow \infty$ , where there is no phase transition, so that we focus on reasonable values of  $N$ . We find that  $T_n$ , in units of  $\rho$ , has a very mild dependence on  $u$ , and thus on  $\rho$  itself, whereas it is very sensitive to  $N$  and  $\lambda_1$ . This is manifest in Fig. 2 (left panel) which shows  $T_n/\rho$  as a function of  $\lambda_1$  for  $N = 10, 15, 25$  and  $\rho = 1, 100$  TeV. The small shift between the dashed and solid curves precisely comes from varying  $\rho$ . For all inputs but  $N$  fixed,  $T_n/\rho$  decreases with increasing  $N$  until reaching a critical value of  $N$  above which the phase transition does not happen. A similar upper bound on  $\lambda_1$  arises when all inputs but  $\lambda_1$  are unchanged. We stress that  $O(4)$  is a good symmetry only for bubbles with critical radius  $R_c < 1/T_n$ . This condition is satisfied whenever the  $O(4)$  solution dominates, for which we find  $R_c T_n \lesssim 0.5$ . Moreover, for the SGWB profiles discussed in the next section, the Big Bang Nucleosynthesis (BBN) bound [7, 27] turns out to require in practice  $T_n/\rho \gtrsim 3 \cdot 10^{-4} \sqrt{N}$ . The degree of supercooling for nucleation temperatures  $T_n \ll T_c$  may trigger a brief period of cosmological inflation. We compute the temperature at which inflation starts,  $T_i$ , by imposing the condition that the energy density in the deconfined phase,  $\rho_d = E_0 + 3\pi^4 \ell^3 T^4/\kappa^2 + \pi^2 g_d^{\text{eff}} T^4/30$ , be dominated by the vacuum energy  $E_0$ . This gives  $T_i \simeq T_c [3 + 4g_d^{\text{eff}}(T_n)/15N^2]^{-1/4}$ . The number of e-folds of inflation produced in the deconfined phase before the transition amounts to  $N_e = \log(T_i/T_n)$  provided that  $T_i > T_n$ . In Fig. 2 (left panel) we plot  $T_i/\rho$  only for  $N = 25$ , while the  $N$ -dependence of  $T_i$  is tiny. In most of the considered parameter space the supercooling triggers a few e-folds of inflation at most.

After the phase transition, the energy density in the deconfined phase  $\rho_d$  is converted into radiation density in the confined phase, and the temperature goes up to the reheat temperature  $T_R$ . The requirement  $\rho_c(T_R) = \pi^2 g_c^{\text{eff}} T^4/30 \simeq \rho_d(T_n)$  implies

$$\frac{4}{15N^2} g_c^{\text{eff}} T_R^4 = T_c^4 + \left( 3 + \frac{4}{15N^2} g_d^{\text{eff}} \right) T_n^4. \quad (17)$$

The reheating is not huge as Fig. 2 (left panel) highlights.

*Gravitational waves.* A cosmological first order phase transition produces a SGWB whose power spectrum  $\Omega_{\text{GW}}(f)$  depends on the dynamics of the bubbles and their interactions with the plasma [5, 28]. When

<sup>1</sup> This approximation holds e.g. in setups with the right-handed top and Higgs localized on the IR brane and the remaining Standard Model fermions elementary. Indeed in the energy budget the difference between  $g_d^{\text{eff}}(T_c) = 97.5$  and  $g_c^{\text{eff}}(T_c) = 106.75$  is negligible as compared to  $45N^2/4$ .

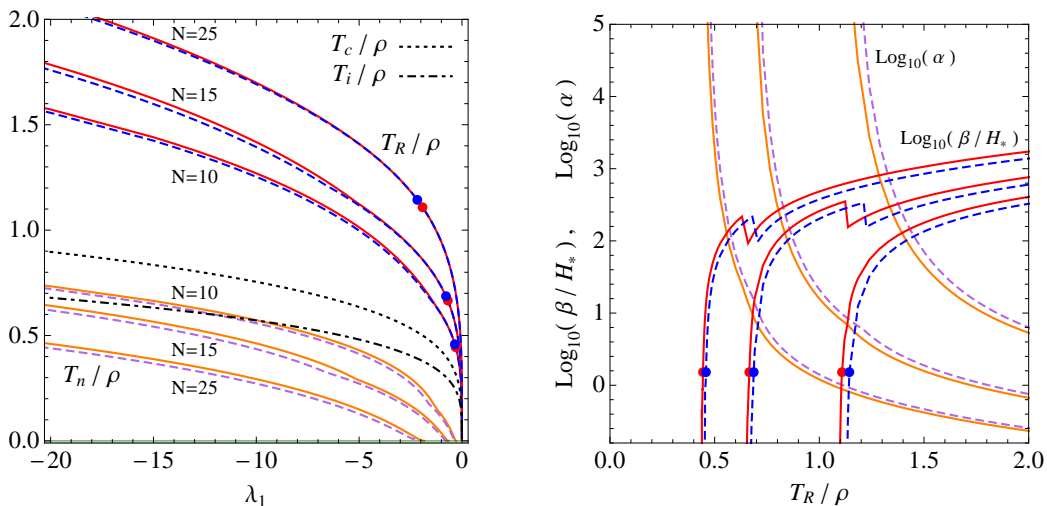


FIG. 2. Left panel:  $T_n/\rho$  (lower set of curves),  $T_R/\rho$  (upper set of curves),  $T_c/\rho$  (dotted black curve) and  $T_i/\rho$  (dashed-dotted black curve) as a function of  $\lambda_1$  for different values of  $N$  and  $\rho$ . Right panel:  $\beta/H_*$  (red and blue curves) and  $\alpha$  (orange and purple curves) as a function of  $T_R/\rho$  for different values of  $N$  and  $\rho$  (curves from left to right are for  $N = 10, 15$  and  $25$ ). Solid (dashed) lines correspond to the cases  $\rho = 1$  TeV (100 TeV) in both panels. The circles correspond to the values on the border of the BBN bound displayed in Fig. 3.

the plasma effects are negligible,  $\Omega_{\text{GW}}(f)$  behaves as  $\Omega_{\text{GW}}^{\text{env}}(f) \simeq 3.8 x^{2.8}/(1+2.8 x^{3.8}) \bar{\Omega}_{\text{GW}}^{\text{env}}$  [29, 30], whereas as  $\Omega_{\text{GW}}^{\text{sw}}(f) \simeq x^3 [7/(4+3x^2)]^{7/2} \bar{\Omega}_{\text{GW}}^{\text{sw}}$  [31–33] in the opposite regime. (Here  $\bar{\Omega}_{\text{GW}}^{\text{env,sw}}$ ,  $f$ , and  $f_p$  are the amplitude, frequency, and peak frequency of the power spectrum, and  $x = f/f_p$ .) The plasma effects are unknown for a supercooled radion phase transition (see discussions in [33]), hence we use  $\Omega_{\text{GW}}^{\text{env}}(f)$  and  $\Omega_{\text{GW}}^{\text{sw}}(f)$  to set the theoretical error on our SGWB prediction<sup>2</sup>.

For  $\bar{\Omega}_{\text{GW}}^{\text{env}}$ ,  $\bar{\Omega}_{\text{GW}}^{\text{sw}}$ , and  $f_p$ , we use the expressions provided in [5, 33]. They depend on: the normalized gap between the free energies in the two phases,  $\alpha = |F_d(T_n) - F_c(T_n)|/\rho_d^*(T_n)$ ; the normalized inverse time duration  $\beta/H_* = T dS_E/dT|_{T=T_n}$ ; and the wall velocity  $v_w$ . The smaller  $\beta/H_*$  and larger  $\alpha$ , the stronger the phase transition and the SGWB signal. For very strong phase transitions one expects  $v_w$  much larger than the sound speed.

Fig. 2 (right panel) shows  $\alpha$  and  $\beta/H_*$  as functions of  $T_R/\rho$  for the aforementioned input values. From these numerical findings we estimate the SGWB signals constituting the theoretical predictions on  $\Omega_{\text{GW}}(f)$  in our setup. Such predictions define the diagonal strips in Fig. 3. The peak amplitude and frequency in the  $\Omega_{\text{GW}}^{\text{env}}$  and  $\Omega_{\text{GW}}^{\text{sw}}$  approximations mark the diagonal lower and upper limits, respectively. The borders are displayed for  $v_w = 0.99$  but no significant change would be visible for e.g.  $v_w \simeq 0.7$ . The strips are cut in their lower part when  $T_R \lesssim 2\rho$  which also yields  $|\delta|/\bar{r}_1^m \lesssim 0.1$ . This prevents

the (large) detuning from jeopardizing our perturbative expansions and suppresses the resonances in the relativistic plasma.

Fig. 3 includes the sensitivity prospects to the parameter space  $\{\bar{\Omega}_{\text{GW}}, f_p\}$  in the  $\Omega_{\text{GW}}^{\text{env}}$  and  $\Omega_{\text{GW}}^{\text{sw}}$  approximations. It displays the situation expected towards the end of the next decade when LISA, ET and aLIGO will have run for several years. For concreteness, the sensitivity regions assume 3, 7 and 8 years of usable data for LISA, ET and aLIGO Design, respectively [37–39]. The exclusion bounds from BBN [7, 27] and aLIGO O2 [40] are also recast. The former varies very little for the  $\Omega_{\text{GW}}^{\text{env}}(f)$  or  $\Omega_{\text{GW}}^{\text{sw}}(f)$  frequency shapes. The latter is based on null searches for signals with signal-to-noise ratio  $\text{SNR} \geq 2$ . Thus, the future sensitivity regions are forecast adopting  $\text{SNR} \geq 2$  and the noise curves of [37–39] (see [41–43] for shortcuts or other approaches).

The forecast shows that by the late 2040s the planned interferometer network will test a huge parameter region, probing  $\rho$  up to the  $10^9$ -TeV scale. Thanks to the complementary of the network, the theoretical uncertainty on the plasma effects during the transition marginally affects the parameter reach of the whole network. The uncertainty is instead relevant in the next years when only aLIGO operates, e.g. aLIGO Design reaches scenarios with  $\rho \sim 100$  TeV only in the  $\Omega_{\text{GW}}^{\text{env}}(f)$  regime.

At qualitative level our findings should apply to any warped setups with radion stabilization mechanism. Such scenarios are indeed expected to have a SGWB phenomenology similar to that here studied. We find that aLIGO O2 data corners vanilla warped scenarios with  $\rho \sim 10^5$  TeV and extremely strong phase transitions.

**Conclusions.** We have analyzed warped models with the radion stabilized by a polynomial potential in the

<sup>2</sup> The turbulence contribution [34, 35] and the different high- $f$  behavior inferred in [36] fall within this theoretical uncertainty.

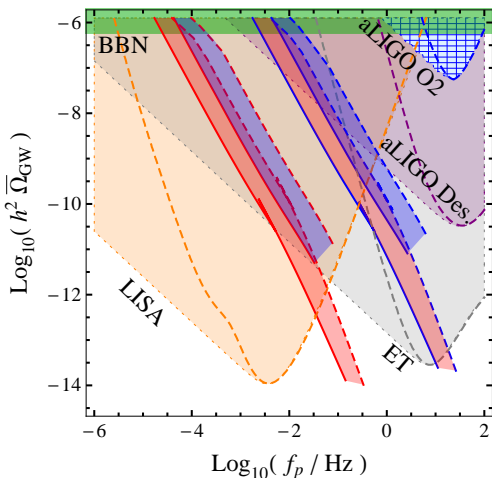


FIG. 3. *Parameter reach in the  $\{h^2\bar{\Omega}_{GW}, f_p\}$  plane for SGWBs in the regimes  $\Omega_{GW}^{\text{env}}$  (regions inside dashed borders) and  $\Omega_{GW}^{\text{sw}}$  (regions inside dotted borders). Diagonal strips are for  $N = 10$  (red) and  $25$  (blue) for  $\rho = 1 \text{ TeV}$  (left set) and  $\rho = 100 \text{ TeV}$  (right set). Solid and dashed lines on the edge of the strips correspond to the regime  $\bar{\Omega}_{GW} \simeq \bar{\Omega}_{GW}^{\text{env}}$  and  $\bar{\Omega}_{GW}^{\text{sw}}$ , respectively. Regions inside the aLIGO O2 and BBN areas are in tension with current data.*

regime of small and sizable backreaction. We have studied the radion phase transition and forecast the detection prospects for the SGWB that the transition produces. We have found that in the next decade the gravitational wave detectors will broadly probe warped models.

We expect our results are generic. Indeed the radion phase transition of the considered model is similar to the one of many other warped setups of the literature. This implies that in all these models the region with

KK resonances at  $m_{\text{KK}} \sim \mathcal{O}(10^5) - \mathcal{O}(10^6) \text{ TeV}$  is being cornered by current aLIGO O2 data. Moreover, the forthcoming interferometers will test models with resonances of mass  $m_{\text{KK}} \lesssim 10^5 \text{ TeV}$  (LISA),  $10^2 \text{ TeV} \lesssim m_{\text{KK}} \lesssim 10^8 \text{ TeV}$  (aLIGO Design) and  $m_{\text{KK}} \lesssim 10^9 \text{ TeV}$  (ET). In this sense, the future gravitational wave detectors have the great potential to shed light on the little hierarchy problem and the amount of tuning that is acceptable in nature.

## ACKNOWLEDGMENTS

The authors thank the ICTP South American Institute for Fundamental Research (SAIFR), Sao Paulo, Brazil, and its Program on Particle Physics, September 30-November 30, 2019, where part of this work was done, for hospitality. The work of EM is supported by the Spanish MINEICO under Grant FIS2017-85053-C2-1-P, by the FEDER Andalucía 2014-2020 Operational Programme under Grant A-FQM-178-UGR18, by Junta de Andalucía under Grant FQM-225, and by Consejería de Conocimiento, Investigación y Universidad of the Junta de Andalucía and European Regional Development Fund (ERDF) under Grant SOMM17/6105/UGR. The research of EM is also supported by the Ramón y Cajal Program of the Spanish MINEICO under Grant RYC-2016-20678. The work of MQ is partly supported by Spanish MINEICO under Grant FPA2017-88915-P, by the Catalan Government under Grant 2017SGR1069, and by Severo Ochoa Excellence Program of MINEICO under Grant SEV-2016-0588.

- 
- [1] L. Randall and R. Sundrum, *Phys. Rev. Lett.* **83**, 3370 (1999), arXiv:hep-ph/9905221 [hep-ph].
- [2] W. D. Goldberger and M. B. Wise, *Phys. Rev. Lett.* **83**, 4922 (1999), arXiv:hep-ph/9907447 [hep-ph].
- [3] A. M. Sirunyan *et al.* (CMS), *JHEP* **04**, 031 (2019), arXiv:1810.05905 [hep-ex].
- [4] M. Aaboud *et al.* (ATLAS), *Phys. Rev. D* **99**, 092004 (2019), arXiv:1902.10077 [hep-ex].
- [5] C. Caprini *et al.*, *JCAP* **1604**, 001 (2016), arXiv:1512.06239 [astro-ph.CO].
- [6] N. Bartolo *et al.*, *JCAP* **1612**, 026 (2016), arXiv:1610.06481 [astro-ph.CO].
- [7] C. Caprini and D. G. Figueroa, *Class. Quant. Grav.* **35**, 163001 (2018), arXiv:1801.04268 [astro-ph.CO].
- [8] P. Creminelli, A. Nicolis, and R. Rattazzi, *JHEP* **03**, 051 (2002), arXiv:hep-th/0107141 [hep-th].
- [9] L. Randall and G. Servant, *JHEP* **05**, 054 (2007), arXiv:hep-ph/0607158 [hep-ph].
- [10] G. Nardini, M. Quiros, and A. Wulzer, *JHEP* **09**, 077 (2007), arXiv:0706.3388 [hep-ph].
- [11] T. Konstandin, G. Nardini, and M. Quiros, *Phys. Rev. D* **82**, 083513 (2010), arXiv:1007.1468 [hep-ph].
- [12] T. Konstandin and G. Servant, *JCAP* **12**, 009 (2011), arXiv:1104.4791 [hep-ph].
- [13] D. Bunk, J. Hubisz, and B. Jain, *Eur. Phys. J. C* **78**, 78 (2018), arXiv:1705.00001 [hep-ph].
- [14] B. M. Dillon, B. K. El-Menoufi, S. J. Huber, and J. P. Manuel, *Phys. Rev. D* **98**, 086005 (2018), arXiv:1708.02953 [hep-th].
- [15] B. von Harling and G. Servant, *JHEP* **01**, 159 (2018), arXiv:1711.11554 [hep-ph].
- [16] S. Bruggisser, B. Von Harling, O. Matsedonskyi, and G. Servant, *Phys. Rev. Lett.* **121**, 131801 (2018), arXiv:1803.08546 [hep-ph].
- [17] S. Bruggisser, B. Von Harling, O. Matsedonskyi, and G. Servant, *JHEP* **12**, 099 (2018), arXiv:1804.07314 [hep-ph].
- [18] E. Megias, G. Nardini, and M. Quiros, *JHEP* **09**, 095 (2018), arXiv:1806.04877 [hep-ph].
- [19] P. Baratella, A. Pomarol, and F. Rompineve, *JHEP* **03**, 100 (2019), arXiv:1812.06996 [hep-ph].
- [20] K. Fujikura, Y. Nakai, and M. Yamada, *JHEP* **02**, 111

- (2020), [arXiv:1910.07546 \[hep-ph\]](#).
- [21] O. DeWolfe, D. Z. Freedman, S. S. Gubser, and A. Karch, *Phys. Rev.* **D62**, 046008 (2000), [arXiv:hep-th/9909134 \[hep-th\]](#).
- [22] I. Papadimitriou, *JHEP* **05**, 075 (2007), [arXiv:hep-th/0703152 \[hep-th\]](#).
- [23] E. Megias and O. Pujolas, *JHEP* **08**, 081 (2014), [arXiv:1401.4998 \[hep-th\]](#).
- [24] J. M. Lizana, M. Olechowski, and S. Pokorski, (2019), [arXiv:1911.11124 \[hep-ph\]](#).
- [25] E. Megias, O. Pujolas, and M. Quiros, *JHEP* **05**, 137 (2016), [arXiv:1512.06106 \[hep-ph\]](#).
- [26] E. Witten, *Adv. Theor. Math. Phys.* **2**, 505 (1998), [arXiv:hep-th/9803131 \[hep-th\]](#).
- [27] R. H. Cyburt, B. D. Fields, K. A. Olive, and E. Skillman, *Astropart. Phys.* **23**, 313 (2005), [arXiv:astro-ph/0408033 \[astro-ph\]](#).
- [28] J. R. Espinosa, T. Konstandin, J. M. No, and G. Servant, *JCAP* **1006**, 028 (2010), [arXiv:1004.4187 \[hep-ph\]](#).
- [29] S. J. Huber and T. Konstandin, *JCAP* **0809**, 022 (2008), [arXiv:0806.1828 \[hep-ph\]](#).
- [30] D. J. Weir, *Phys. Rev.* **D93**, 124037 (2016), [arXiv:1604.08429 \[astro-ph.CO\]](#).
- [31] M. Hindmarsh, S. J. Huber, K. Rummukainen, and D. J. Weir, *Phys. Rev.* **D92**, 123009 (2015), [arXiv:1504.03291 \[astro-ph.CO\]](#).
- [32] M. Hindmarsh, S. J. Huber, K. Rummukainen, and D. J. Weir, *Phys. Rev. D* **96**, 103520 (2017), [Erratum: *Phys. Rev. D* 101, 089902 (2020)], [arXiv:1704.05871 \[astro-ph.CO\]](#).
- [33] C. Caprini *et al.*, *JCAP* **2003**, 024 (2020), [arXiv:1910.13125 \[astro-ph.CO\]](#).
- [34] C. Caprini, R. Durrer, and G. Servant, *JCAP* **0912**, 024 (2009), [arXiv:0909.0622 \[astro-ph.CO\]](#).
- [35] T. Kahniashvili, L. Kisslinger, and T. Stevens, *Phys. Rev.* **D81**, 023004 (2010), [arXiv:0905.0643 \[astro-ph.CO\]](#).
- [36] D. Cutting, M. Hindmarsh, and D. J. Weir, *Phys. Rev.* **D97**, 123513 (2018), [arXiv:1802.05712 \[astro-ph.CO\]](#).
- [37] H. Audley *et al.*, (2017), [arXiv:1702.00786 \[astro-ph.IM\]](#).
- [38] B. Sathyaprakash *et al.*, *Class. Quant. Grav.* **29**, 124013 (2012), [Erratum: *Class. Quant. Grav.* 30, 079501 (2013)], [arXiv:1206.0331 \[gr-qc\]](#).
- [39] B. P. Abbott *et al.* (VIRGO, LIGO Scientific), (2013), [10.1007/lrr-2016-1](#), [Living Rev. Rel. 19, 1 (2016)], [arXiv:1304.0670 \[gr-qc\]](#).
- [40] B. Abbott *et al.* (LIGO Scientific, Virgo), *Phys. Rev. D* **100**, 061101 (2019), [arXiv:1903.02886 \[gr-qc\]](#).
- [41] C. Caprini, D. G. Figueroa, R. Flauger, G. Nardini, M. Peloso, M. Pieroni, A. Ricciardone, and G. Tasinato, *JCAP* **11**, 017 (2019), [arXiv:1906.09244 \[astro-ph.CO\]](#).
- [42] D. J. Weir *et al.* (LISA CosWG), “PTPlot webpage,” <http://www.ptplot.org/ptplot>.
- [43] K. Schmitz, [arXiv:2002.04615 \[hep-ph\]](#).